

Effect of confining FRP overlays on bond strength enhancement

Sevket Ozden ^{*}, Erkan Akpinar

Department of Civil Engineering, Kocaeli University, Kocaeli 41040, Turkey

Received 18 January 2006; received in revised form 26 July 2006; accepted 1 August 2006

Available online 28 September 2006

Abstract

In this study, changes in the bond strength of reinforcing bars due to external confinement, through FRP overlays, was investigated. Eccentric pullout specimens with insufficient bond length and with two different normal strength concrete levels were reinforced with single deformed bars placed with a small cover thickness. Three reinforcing bar sizes and two FRP types, each having two different number of layers, were used in the experiments. Significant enhancement in bond strength due to FRP confinement was observed in all specimens. Although the increase in bond strength was closely related to the clamping force developed by the FRP overlays, the effectiveness of the invoked clamping force reduces beyond a limiting value. The orientation of the splitting cracks was also affected by the existence of the FRP overlays.

© 2006 Elsevier Ltd. All rights reserved.

Keywords: Bond strength; Reinforced concrete; Normal strength concrete; Confinement; Carbon fiber reinforced polymer (CFRP); Glass fiber reinforced polymer (GFRP)

1. Introduction

The bond mechanism and the parameters affecting the bond strength between reinforcing bars and the concrete are commonly defined and cataloged by the researchers of the recent century [1–6]. Parameters affecting the bond strength may be summarized into three major groups as follows. Components of the concrete mix, such as the types of aggregates, binding minerals, fibers, admixtures, and the level of concrete strength, both compressive and tensile, may be accounted as the first group of parameters [1,5,7–20]. The second group, which is mainly associated with the reinforcing bar itself, may be listed as reinforcing bar diameter, rib geometry and reinforcing bar surface specifications, splice length, position of the reinforcing bars with respect to each other and to concrete surface, and the reinforcing bar surface coating [1,2,4,9,16–18,21–26]. The rest of the influencing parameters may be classified in the third group and may be listed as the existence and amount of transverse rein-

forcement, lateral pressure, temperature, corrosion level, environmental conditions, and the loading history, etc. [4,8,14,18,24,25,27–30].

Bond stress that leads the concrete and reinforcing steel to work together is the result of an interaction between the reinforcing bar and the concrete placed around it. The main part of this interaction may be defined as the mechanical bond stresses in the case of deformed reinforcing bars. The pseudo-concrete-cylinder (PCC) which is placed around the reinforcing bar, with a diameter bordered with the minimum of concrete cover or half of the bar spacing, controls the bond action and the bond failure basically. The mechanical bond stresses developed in case of deformed reinforcing bars yields radial stress components, depending on the rib geometry and rib angle, that causes tensile stresses in the so called PCC and tries to split it to failure [2–4,6]. Delaying the tensile splitting of PCC or totally preventing it enhances the bond strength and may well be succeeded by using transverse steel around the reinforcing bars, or by increasing the tensile strength of the concrete matrix by using higher strength concrete. On the other hand, it should be noted that, the shearing of con-

^{*} Corresponding author. Tel.: +90 532 744 3921; fax: +90 262 335 5381.
E-mail address: sevketozden@yahoo.com (S. Ozden).

Notation

C	concrete cover thickness (mm)	P	tension force on the reinforcing bar applied by the hydraulic jack
C_s	rib spacing (mm)	t_{FRP}	thickness of FRP overlay (one ply) (mm)
D_b	reinforcing bar diameter (mm)	u_c	calculated average bond stress at failure (MPa)
E_{Comp}	modulus of elasticity of composite (FRP and epoxy) (MPa)	u_e	measured average bond stress at failure (MPa)
E_{Epoxy}	modulus of elasticity of epoxy resin (MPa)	u_{eo}	measured average bond stress at failure in virgin specimens (MPa)
E_{FRP}	modulus of elasticity of FRP overlay (MPa)	V	vertical support forces (kN)
E_s	modulus of elasticity of reinforcing bar (MPa)	VP_{Epoxy}	volume percent of epoxy resin in epoxy–FRP composite (%)
f'_c	compressive strength of concrete (150×300 mm cylinder) (MPa)	VP_{FRP}	volume percent of FRP in epoxy–FRP composite (%)
f'_{cn}	nominal compressive strength of concrete (MPa)	w	cross-sectional width of the specimen (mm)
f'_{cs}	split cylinder strength of concrete (150 × 300 mm cylinder) (MPa)	σ_{CSCc}	calculated clamping stress on PCC (MPa)
F_R	rib area (mm ²)	$\sigma_{CSCc-lim}$	limit value for the calculated clamping stress on PCC (MPa)
f_y	yield strength of reinforcing bar (MPa)	σ_{CSCe}	measured clamping stress on PCC (MPa)
h	cross-sectional height of the specimen (mm)	σ_{FRPe}	measured average stress in FRP at the time of bond failure (MPa)
k	number of ribs at cross-section of the bar	$\Delta(u_c/f'_c)^{(1/2)}$	normalized bond strength enhancement
k_1	aspect coefficient for bond effectiveness (considers perimeter/area relation)	α	rib inclination to bar axis (°)
l_b	bond length (mm)	β	rib face angle (°)
L_{SR}	gauge length of strain readings on FRP parallel to fiber orientation (mm)	ϵ_{co}	concrete tensile strain at the time of bond failure
m_1	initial slope of the idealized effectiveness of FRP clamping on bond strength	ϵ_{FRPe}	calculated FRP strain at the time of bond failure
m_2	secondary slope of the idealized effectiveness of FRP clamping on bond strength	ϵ_{FRPe}	measured FRP strain at the time of bond failure
n	number of FRP layer	PCC	pseudo-concrete-cylinder
		RRA	relative rib area

crete lugs between the ribs of reinforcement along the reinforcing bar axis is another limit for the bond failure.

Available literature on the subject reveals that higher strength concrete classes provide higher tensile strength, hence resulting improvement in bond strength. On the other hand, the increase in tensile strength of concrete beyond a certain compressive strength level is so small that the bond strength may not be improved further [10,16,18,26]. In addition, the bond stress distribution along the reinforcing bar axis becomes more non-uniform and fewer lugs participate in the stress transform in the case of higher concrete strength classes [15,18]. The use of steel fibers in the concrete matrix is reported to increase the tensile strength and toughness of concrete, resulting in a higher bond strength and leading to a considerable improvement in ductility of bond slip behavior especially for the cases of splitting predominant failures; through delaying the splitting failures [6,12–14,19]. Higher bond strengths may be obtained for higher ratios of steel fibers in concrete.

The ratio of wall thickness of the PCC surrounding the reinforcing bar, to the reinforcing bar diameter (C/D_b) is observed as another parameter affecting the

bond strength. It was reported that, lower C/D_b values results in lower bond strength values [21]. On the other hand, sustained increases in C/D_b beyond a certain limit does not result in bond strength increase since the failure mechanism changes from splitting of PCC towards the pullout of reinforcing bar. This limiting value is reported between 2.5 and 3 in the available literature [4,25].

Confinement on the concrete section, either active or passive, has significant positive contribution on the bond strength [6,25]. It can be concluded from the results of many researchers that the use of transverse reinforcement in reinforced concrete members causes higher bond strength levels and more ductile bond behavior; leading to sufficient bond strength with a relatively shorter anchorage length [4,6,8,18,27,29,30]. Likely the effects of concrete cover thickness, sustained increases in confinement may not result in further bond strength increases since the failure mode is changed from splitting to pullout. Some of the recent investigations indicated that FRP wrapped concrete beams were upgraded by means of not only significant improvements in load capacity and ductility but also considerable enhancement on bond performance [31–33].

2. Experimental procedure

Insufficient anchorage length in flexural members generally results in brittle and premature failures triggered by inadequate bond strength. The anchorage length may be considered as insufficient due either to a lower concrete strength, higher reinforcing steel yield strength, small concrete cover thickness, or small anchorage length relative to the design specified values, and the external FRP confining overlays may well be a solution in the case of such deficiencies. This study highlights the effectiveness of bond strength improvement and attainable level of bond strength increase by the use of FRP confining overlays.

2.1. Test specimens

Seventy H-shaped eccentric pullout specimens (Fig. 1) with insufficient bond length, l_b were designed and constructed in this study [34]. The H-shaped specimens which have rectangular cross-section at the testing region ($w = 240$ mm; $h = 300$ mm) were intended to simulate the bond in a reinforced concrete member under combined flexure and shear forces (Fig. 1). In order not to trigger a shear failure before reaching the bond strength of the sub-assembly, the length of the member was designed longer than the bond length. No longitudinal or transverse reinforcement, except the specific reinforcing bar for the bond test, was used in any of the H-shaped specimens.

Two different concrete nominal compressive strength levels, namely $f'_{cn} = 20$ MPa and $f'_{cn} = 40$ MPa, were used in the test specimens. It was intended to obtain data for the normal strength concrete (NSC) range which is common in the existing building and bridge stock. Three different bar diameters (D_b) were used in each concrete strength level. The cross-sectional area over perimeter ratio for the $D_b = 12$ mm, $D_b = 16$ mm and $D_b = 26$ mm reinforcing bars were 3.0, 4.0 and 6.5, respectively. The reinforcing bars were placed at the bottom of the cross-section (bottom cast bars) during casting. For each combination of concrete quality and reinforcing bar diameter, two different FRP

types, namely CFRP and GFRP, were used with two different number of layers. The FRP overlays were used only over the bonded length, l_b and the fiber orientation of the FRP layers were perpendicular to the reinforcing bar axis. In each set, two specimens were tested without FRP overlay. The concrete cover thickness over reinforcing bar diameter ratio (C/D_b) was kept at unity in all specimens.

The specimens were named in a way to recognize the variables tested in this specific specimen. The first four letters in the specimen names give the nominal concrete strength in MPa. The next three letters show the diameter of reinforcing bar in millimeters. The third info block with three letters shows the polymer type and the number of layer of the confining FRP overlay. And the last variable block was used to distinguish the replicas of the specimens with the same variable list. The first specimen with 20 MPa concrete strength and 26 mm bar diameter, confined with 4 layers of CFRP was named as EC20D26-FC4-A while the second specimen of the same set was called as EC20D26-FC4-B.

2.2. Material properties

Portland cement, river sand and crushed limestone were used in the concrete mix. The water cement ratios for $f'_{cn} = 20$ MPa and $f'_{cn} = 40$ MPa concrete classes were 0.8 and 0.48, respectively. A commercially available superplasticizer conforming to ASTM C494-81-F specifications was used in the $f'_{cn} = 40$ MPa concrete at an amount equal to 2% of the cement weight. Vibration was applied to all specimens for regular compaction of concrete. The development of concrete compressive strength over time was monitored by compression tests on 150×300 mm cylinders. Concrete compressive strength values (f'_{cn}) at the time of sub-assembly testing varied between 19.3 and 24.6 MPa for the $f'_{cn} = 20$ MPa specimen set and between 40.6 and 45.5 MPa for the $f'_{cn} = 40$ MPa specimen set.

The reinforcing bars with 12, 16, and 26 mm nominal diameters (D_b) were tested in a 600 kN capacity universal testing machine, with fully electronic data acquisition, in

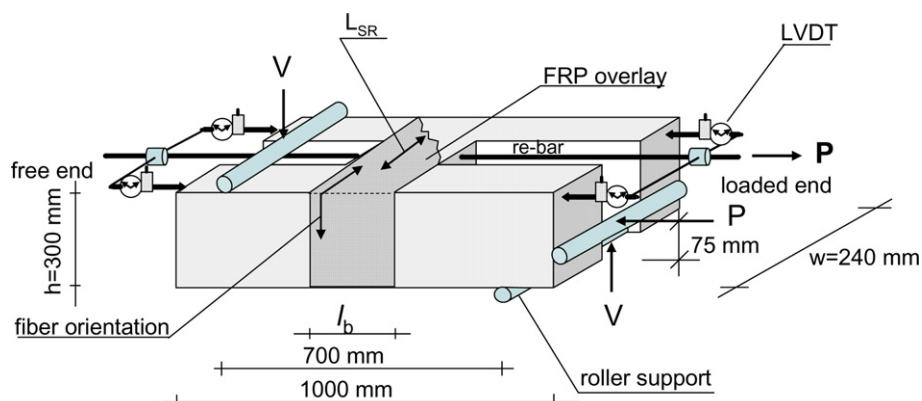
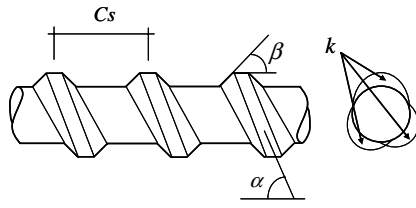


Fig. 1. Specimen dimensions.

Table 1
FRP, epoxy and reinforcing bar properties

Property	FRP and Epoxy		
	CFRP	GFRP	Epoxy
Thickness (mm)	0.117	0.157	N/A
Modules of Elasticity (MPa)	240,000	73,000	6000
Tensile strength (MPa)	3800	3400	17
Fiber density (g/m ³)	1.70	2.54	N/A
Fiber area weight (g/m ²)	200	400	N/A
Ultimate elongation (%)	1.58	4.66	N/A
Adhesion to concrete (MPa)	N/A	N/A	4
	Reinforcing bar		
	$D_b = 12$ mm	$D_b = 16$ mm	$D_b = 26$ mm
Nominal bar diameter (mm)	12	16	26
Modules of Elasticity (MPa)	195,000	194,400	195,100
Yield Strength (MPa)	495	510	540
No. of ribs at the x -section, k	3	3	3
Area of one rib, F_R (mm ²)	6.57	13.29	33.44
Rib angle, α (°)	53.0	50.8	50.7
Rib face angle, β (°)	46.3	47.0	48.2
Rib spacing, C_s (mm)	7.46	10.98	15.84
Relative rib area (RRA)	0.056	0.056	0.060
	$RRA = \frac{kF_R \sin \alpha}{\pi D_b C_s}$		



order to clearly define the modulus of elasticity (E_s) and the yield strength (f_y) (Table 1). The rib geometry of the reinforcing bars also were measured and listed in Table 1 with reference to Fig. 1. All three reinforcing bars can be classified as high relative rib area reinforcing bars good for high bond strength.

The CFRP and GFRP fabrics used in this investigation were unidirectional and with continuous fiber forms. The manufacturer specified material properties of FRP fabrics and the epoxy resin are presented in Table 1.

2.3. Strengthening of specimens

The same FRP application procedure was used in all strengthened test specimens. Special consideration was given to the surface and corner preparation of the specimens before the application of the epoxy glued FRP fabrics. All specimen corners were grinded to a radius of 25 mm before the application of the FRP overlays. Steel wire brushing and air washing was applied to the surface of the specimens to remove the dust and loose particles from the surface.

During the application process of FRP to the specimen surface over the bond length, one layer of epoxy was applied to the specimen surface initially. Later FRP fabrics were placed with an orientation perpendicular to the reinforcing bar axis. Each FRP layer was impregnated with a steel roller and coated with epoxy adhesive. The final overlap length of FRP fabrics were 100 mm. All strengthened specimens were cured in the laboratory for not less than 7 days before the test.

2.4. Test setup and loading history

The H-shaped eccentric pullout specimens (Fig. 1) were tested horizontally in a specially designed test setup. The tension force on the reinforcing bar (P) was applied by two hollow type, manually driven hydraulic jacks seated on either end of the protruding reinforcing bar, and the level of the force was measured by two 100 kN capacity load cells. Reversed tension–unload–tension type of loading scheme on either end of the reinforcing bar was applied to all specimens. Three reversed load cycles were made at 10%, 20%, 30% and 40% load levels of the specimen's calculated bond capacity. The nominal bond strength for all specimens was calculated as $2f_{cn}^{(1/2)}$ and the test load P was calculated by the product of the nominal bond strength and the bonded surface area of the reinforcing bar. All specimens were loaded to failure after the 40% load cycle.

The test specimens were fixed horizontally, and the moment caused by the P force and the horizontal reaction was resisted by the coupling moment created by the vertical support forces, V ; in turn V acts as shear force on the specimen.

Four 30 mm capacity linear variable differential transducers (LVDT) with a sensitivity of 0.01 mm were used to measure the free and loaded end slip values on either ends of the specimens. All displacement and load readings, along with the average strain measurements on the FRP layers (in the direction of fibers) (Fig. 1), were monitored and recorded by an electronic data acquisition system. The average strain measurements on FRP were made by using an LVDT driven clip gauge with a $L_{SR} = 100$ mm gauge length.

3. Experimental observations

3.1. Cracks and failure modes

All specimens reported in this study reached their ultimate failure load mainly through splitting type of bond failure. The strains on the FRP overlays, which was measured perpendicular to the reinforcing bar axis, and reinforcing bar free end slip values reached their maximum right prior to the bond failure.

The splitting cracks on the anchorage region of the specimens without FRP overlays, were unique and aligned with the reinforcing bars (Fig. 2). These cracks were between the reinforcing bar and the specimen's top surface, which

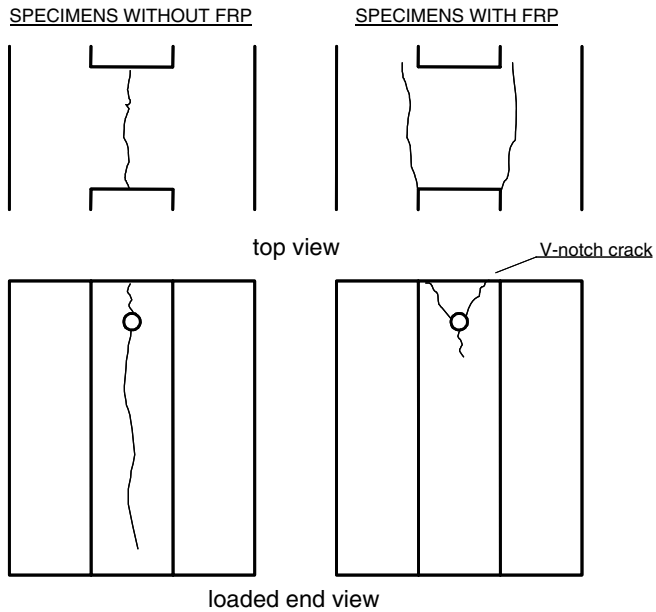


Fig. 2. Splitting failure cracks in specimens.

points out the smallest cover thickness, and were observable at the loaded ends. In addition, V-notch cracks with an approximate V-notch angle of less than 30° were also observed at the free end of these specimens.

On the other hand, two main splitting cracks starting from the reinforcing bar and forming a V-notch at either end were observed on all specimens wrapped with FRP overlays. The angle between the V-notch cracks varied mainly depending on the modulus of elasticity and the total thickness of the FRP overlays; in other words depending on the amount of clamping force generated by the FRP overlay. The splitting cracks observed at the loaded end of the specimen were almost horizontal (V-notch failure surface flattens) for most of the confined specimens. The V-notch angle at the free end also increased with increasing number of layer of FRP overlays.

It was observed that the splitting cracks along the reinforcing bar axis were also traceable through the depth of the specimens that were without FRP overlays. The application of the FRP overlay confined these splitting cracks to the cover region and prevented the expansion and progress of these cracks through the depth of the specimen by changing the crack orientation. It should be noted that the higher the elastic modulus or number of layers of FRP overlays, the confined the cracking to the reinforcing bar periphery (Fig. 2).

Although the effects of conventional transverse reinforcement and the FRP overlays on bond strength enhancement and on splitting crack development are similar, unlike the transverse reinforcement, FRP overlays not only delayed the crack propagation but also altered their orientations from the shortest distance to the surface to a longer concrete path (Fig. 2).

The degradation of pull-out stiffness, which is the slope of the load versus loaded-end-slip graphics, of all

specimens tested under tension–unload–tension type of reversed loading was also investigated [34]. It was observed that the stiffness degradation under reversed loading (loaded maximum to 40% of capacity) was insignificant at approximately service load levels.

3.2. Enhancement in bond stress at failure

The concrete properties (f'_c and f'_{cs}), reinforcing bar diameter (D_b), anchorage length (l_b), type and number of layer (n) of FRP overlay, and the experimentally measured average bond stress at failure (u_e) of all specimens are given in Table 2; where the average bond stress at failure, u_e is calculated according to Eq. (1)

$$u_e = \frac{P}{\pi D_b l_b} \quad (1)$$

The average bond stress at failure, u_e for the specimens with FRP overlays were consistently above their counterpart specimens without FRP (Table 2), regardless of the FRP type and number of layers (n), concrete compressive strength (f'_{cn}), and the reinforcing bar diameter (D_b). When the increase in average bond stress at failure is investigated (Table 3), it is observed that the percent increase in u_e closely depends on the variables listed above. The average enhancement in bond stress at failure, u_e due to FRP overlays for a nominal concrete strength of $f'_{cn} = 20$ MPa was between 16% and 42%, while it was between 18% and 40% for $f'_{cn} = 40$ MPa concrete. The percent enhancement in bond stress at failure is also affected by the bar diameter, in other words the cross-sectional area over perimeter ratio. The average enhancement in bond stress at failure for $D_b = 12$ mm diameter reinforcing bar was 28% while this enhancement was 31.5% and 35% for $D_b = 16$ mm and $D_b = 26$ mm diameter bars, respectively, for $f'_{cn} = 20$ MPa concrete (Table 3). Furthermore, the type of FRP has an influence on the percent increase in the splitting failure load. The difference in modulus of elasticity of GFRP and CFRP, in turn, the difference in the clamping stresses developed under a given strain on the FRP overlay may be the reason for such a difference. Considering the test results, bond strength enhancement through externally applied FRP overlays may well be an easy and effective way on the anchorage or lap splice regions of the flexural members.

The strain values measured on the FRP overlays (ϵ_{FRPe}), perpendicular to the reinforcing bar axis, monitored throughout the test to calculate the tensile stress on FRP composite (σ_{FRPe}) at splitting bond failure load level as shown in Eq. (2) and as given in Table 2, column 8

$$\sigma_{FRPe} = \epsilon_{FRPe} E_{Comp} \quad (2)$$

where the modulus of elasticity of the composite, E_{Comp} is calculated according to Eq. (3), by assuming approximately 50% volume fractions were used both for epoxy and FRP

Table 2
Specimen specifications and test results

	Specimen	(1) f'_c (MPa)	(2) f'_{cs} (MPa)	(3) D_b (mm)	(4) l_b (mm)	(5) FRP type	(6) n	(7) u_e (MPa)	(8) σ_{FRPc} (MPa)	(9) σ_{CSCc} (MPa)
1	EC20D12-F00-A	21.3	2.18	12	84	–	–	9.46	–	–
2	EC20D12-F00-B	21.6	2.24	12	84	–	–	10.26	–	–
3	EC20D12-FC2-A	21.3	2.18	12	84	CFRP	2	11.64	189.34	1.23
4	EC20D12-FC2-B	21.6	2.24	12	84	CFRP	2	11.28	234.97	1.53
5	EC20D12-FC4-A	21.3	2.18	12	84	CFRP	4	13.46	312.43	4.06
6	EC20D12-FC4-B	21.6	2.24	12	84	CFRP	4	14.55	181.92	2.36
7	EC20D12-FG3-A	21.3	2.18	12	84	GFRP	3	13.10	92.01	1.20
8	EC20D12-FG3-B	21.6	2.24	12	84	GFRP	3	13.17	54.31	0.71
9	EC20D12-FG5-A	21.3	2.18	12	84	GFRP	5	12.08	51.18	1.12
10	EC20D12-FG5-B	21.6	2.24	12	84	GFRP	5	11.86	62.07	1.35
11	EC20D16-F00-A	21.4	2.17	16	112	–	–	7.61	–	–
12	EC20D16-F00-B	21.6	1.93	16	112	–	–	7.90	–	–
13	EC20D16-FC2-A	21.4	2.17	16	112	CFRP	2	11.75	269.10	1.31
14	EC20D16-FC2-B	21.6	1.93	16	112	CFRP	2	9.99	209.23	1.02
15	EC20D16-FC2-r	19.3	1.99	16	112	CFRP	2	9.78	206.83	1.01
16	EC20D16-FC4-A	21.4	2.17	16	112	CFRP	4	10.23	219.33	2.14
17	EC20D16-FC4-B	21.6	1.93	16	112	CFRP	4	10.97	283.03	2.76
18	EC20D16-FC4-r	19.3	1.99	16	112	CFRP	4	10.23	573.17	5.59
19	EC20D16-FG3-A	21.4	2.17	16	112	GFRP	3	9.50	–	–
20	EC20D16-FG3-B	21.6	1.93	16	112	GFRP	3	8.96	72.02	0.71
21	EC20D16-FG5-A	21.4	2.17	16	112	GFRP	5	11.91	70.46	1.15
22	EC20D16-FG5-B	21.6	1.93	16	112	GFRP	5	9.46	63.72	1.04
23	EC20D16-FG5-r	19.3	1.99	16	112	GFRP	5	10.56	210.04	3.43
24	EC20D26-F00-A	24.6	2.33	26	91	–	–	6.79	–	–
25	EC20D26-F00-B	21.2	2.08	26	91	–	–	6.82	–	–
26	EC20D26-FC2-A	24.6	2.33	26	91	CFRP	2	9.36	306.07	0.92
27	EC20D26-FC2-B	21.2	2.08	26	91	CFRP	2	8.49	188.79	0.57
28	EC20D26-FC4-A	24.6	2.33	26	91	CFRP	4	10.85	615.72	3.69
29	EC20D26-FC4-B	21.2	2.08	26	91	CFRP	4	9.27	574.97	3.45
30	EC20D26-FC4-r	19.3	1.99	26	91	CFRP	4	8.80	436.02	2.62
31	EC20D26-FG3-A	24.6	2.33	26	91	GFRP	3	8.96	151.55	0.92
32	EC20D26-FG3-B	21.2	2.08	26	91	GFRP	3	8.80	111.82	0.68
33	EC20D26-FG5-A	24.6	2.33	26	91	GFRP	5	9.55	116.72	1.17
34	EC20D26-FG5-r	19.3	1.99	26	91	GFRP	5	9.08	119.71	1.20
35	EC40D12-F00-A-r	44.8	3.48	12	42	–	–	12.23	–	–
36	EC40D12-F00-B-r	41.0	3.35	12	42	–	–	11.21	–	–
37	EC40D12-FC2-A	42.1	3.06	12	42	CFRP	2	13.83	361.68	2.35
38	EC40D12-FC2-A-r	44.8	3.48	12	42	CFRP	2	14.99	115.60	0.75
39	EC40D12-FC2-B	45.5	3.29	12	42	CFRP	2	13.54	199.21	1.29
40	EC40D12-FC2-B-r	41.0	3.35	12	42	CFRP	2	15.14	206.17	1.34
41	EC40D12-FC4-A	42.1	3.06	12	42	CFRP	4	14.41	228.98	2.98
42	EC40D12-FC4-A-r	44.8	3.48	12	42	CFRP	4	15.43	264.25	3.44
43	EC40D12-FC4-B	45.5	3.29	12	42	CFRP	4	17.17	164.48	2.14
44	EC40D12-FC4-B-r	41.0	3.35	12	42	CFRP	4	15.72	120.07	1.56
45	EC40D12-FG3-A-r	44.8	3.48	12	42	GFRP	3	15.14	38.22	0.50
46	EC40D12-FG3-B-r	41.0	3.35	12	42	GFRP	3	13.68	47.80	0.63
47	EC40D12-FG5-A	42.1	3.06	12	42	GFRP	5	15.43	101.54	2.21
48	EC40D12-FG5-A-r	44.8	3.48	12	42	GFRP	5	13.24	88.81	1.94
49	EC40D12-FG5-B	45.5	3.29	12	42	GFRP	5	15.28	88.37	1.93
50	EC40D12-FG5-B-r	41.0	3.35	12	42	GFRP	5	14.99	47.54	1.04
51	EC40D16-F00-A	40.6	3.75	16	56	–	–	9.09	–	–
52	EC40D16-F00-B	42.9	3.57	16	56	–	–	10.89	–	–
53	EC40D16-FC2-A	40.6	3.75	16	56	CFRP	2	14.33	225.50	1.10
54	EC40D16-FC2-B	42.9	3.57	16	56	CFRP	2	12.28	225.50	1.10
55	EC40D16-FC4-A	40.6	3.75	16	56	CFRP	4	15.55	264.72	2.58
56	EC40D16-FC4-B	42.9	3.57	16	56	CFRP	4	13.02	238.11	2.32
57	EC40D16-FG3-A	40.6	3.75	16	56	GFRP	3	11.71	58.42	0.57
58	EC40D16-FG3-B	42.9	3.57	16	56	GFRP	3	11.87	92.13	0.90
59	EC40D16-FG5-A	40.6	3.75	16	56	GFRP	5	12.77	76.23	1.25
60	EC40D16-FG5-B	42.9	3.57	16	56	GFRP	5	14.24	73.64	1.20
61	EC40D26-F00-A	43.5	3.32	26	91	–	–	7.60	–	–
62	EC40D26-F00-B	45.2	3.52	26	91	–	–	8.74	–	–
63	EC40D26-FC2-A	43.5	3.32	26	91	CFRP	2	11.59	443.79	1.33

Table 2 (continued)

Specimen	(1) f'_c (MPa)	(2) f'_{cs} (MPa)	(3) D_b (mm)	(4) l_b (mm)	(5) FRP type	(6) n	(7) u_e (MPa)	(8) σ_{FRPe} (MPa)	(9) σ_{CSCc} (MPa)	
64	EC40D26-FC2-B	45.2	3.52	26	91	CFRP	2	11.22	357.42	1.07
65	EC40D26-FC4-A	43.5	3.32	26	91	CFRP	4	11.38	668.04	4.01
66	EC40D26-FC4-B	45.2	3.52	26	91	CFRP	4	11.44	603.29	3.62
67	EC40D26-FG3-A	43.5	3.32	26	91	GFRP	3	10.73	85.37	0.52
68	EC40D26-FG3-B	45.2	3.52	26	91	GFRP	3	10.57	99.74	0.60
69	EC40D26-FG5-A	43.5	3.32	26	91	GFRP	5	11.44	108.03	1.09
70	EC40D26-FG5-B	45.2	3.52	26	91	GFRP	5	11.38	107.20	1.08

Table 3

Increase in average bond stress at failure

f'_{cn} (MPa)	D_b (mm)	FRP type	n (layers)	Increase in u_e (%)	
20	12	CFRP	2	16	
			4	42	
		GFRP	3	33	
			5	21	
		16	CFRP	2	35
				4	35
	GFRP		3	19	
			5	37	
	26	CFRP	2	31	
			4	42	
		GFRP	3	30	
			5	37	
40	12	CFRP	2	23	
			4	34	
		GFRP	3	23	
			5	26	
		16	CFRP	2	33
				4	43
	GFRP		3	18	
			5	35	
	26	CFRP	2	40	
			4	40	
		GFRP	3	30	
			5	40	

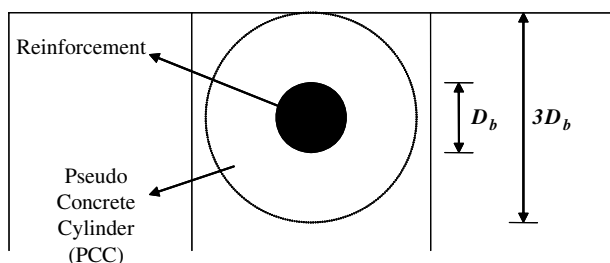


Fig. 3. The pseudo-concrete-cylinder (PCC) around steel reinforcing bar.

during the impregnation and the elastic modulus of FRP and the epoxy resin are given in Table 1

$$E_{Comp} = E_{FRP}VP_{FRP} + E_{Epoxy}VP_{Epoxy} \quad (3)$$

It was observed that the enhancement due to FRP overlays is closely related to the tensile stress in FRP (σ_{FRPe}), hence

related to the clamping stress (σ_{CSCc}) on the pseudo-concrete-cylinder (PCC) (Fig. 3). The clamping stress which was calculated as dividing the clamping force by the product of diameter of PCC and the reinforcing bar anchorage length is given in Eq. (4) and the values are listed in Table 2

$$\sigma_{CSCc} = \frac{\sigma_{FRPe}n l_{FRP}}{3D_b} \quad (4)$$

The relation between the above equation and the attained level of bond strength may be observed from columns 7 and 9 of Table 2. It may be easy to investigate this relation by grouping the results with respect to re-bar diameter for each concrete level. As an example, the bond stress, u_e and the clamping stress, σ_{CSCc} in specimen EC20D12-FC4-A were 13.46 MPa and 4.06 MPa, respectively, while these values were 13.10 MPa and 1.20 MPa for specimen EC20D12-FG3-A. Although the change in clamping stress was above three folds between these two specimens, the change in bond strength enhancement was negligible. Similar trend was observed also in other reinforcement diameter groups. It should be noted that the diminishing effectiveness of increasing overlay thickness and elastic modulus may highlight a change in failure mode.

3.3. Effectiveness of FRP overlays

The relationship between the normalized average bond stress at failure (u_e/f'_c) and the clamping stress on the pseudo-concrete-cylinder (σ_{CSCc}), calculated according to Eq. (4), is presented in Figs. 4 and 5 for $f'_{cn} = 20$ MPa and $f'_{cn} = 40$ MPa concrete specimens, respectively. It is observed that the increasing clamping stresses on PCC resulted in an increase in the normalized average bond stress at failure (u_e/f'_c). It should be pointed out that, after a certain clamping stress level the bond strength enhancement takes place at a slower pace rate. This critical level of clamping stress is called the limiting clamping stress on PCC ($\sigma_{CSCc-lim}$) and it points out the boundary of gradual change in bond failure mode. As it is pointed out by the previous researchers [25,29], the modes of bond failure are bounded by two extremes, namely splitting and pull-out failures. In case of small confining pressures the failure is mainly splitting type, while heavy confinement or the lack of ribs on the reinforcing bars lead to a pull-out type (shearing the con-

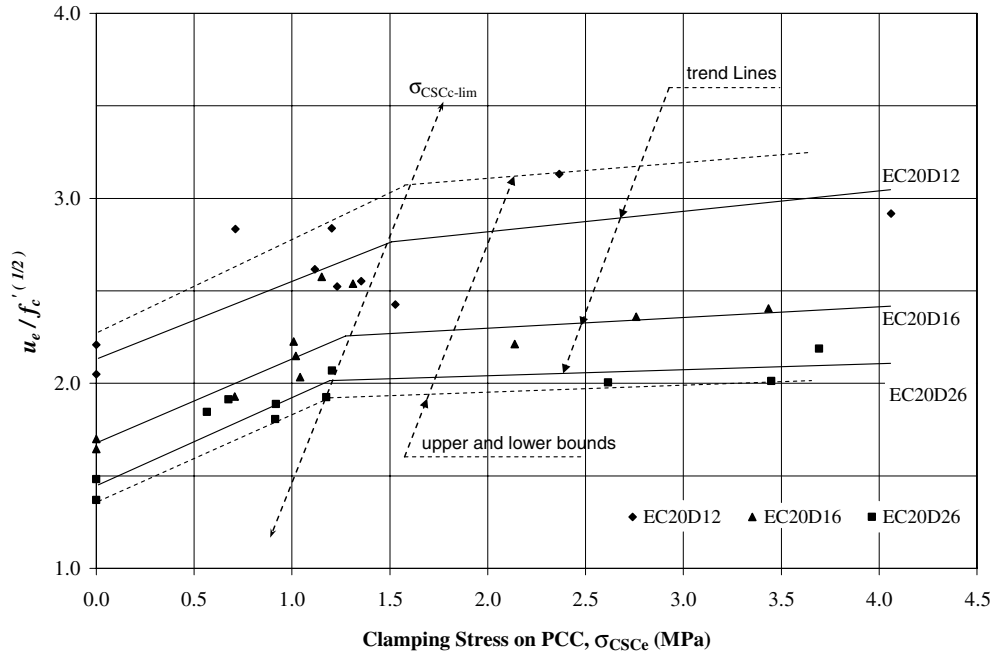


Fig. 4. Normalized bond strength versus clamping stress ($f'_{cn} = 20$ MPa).

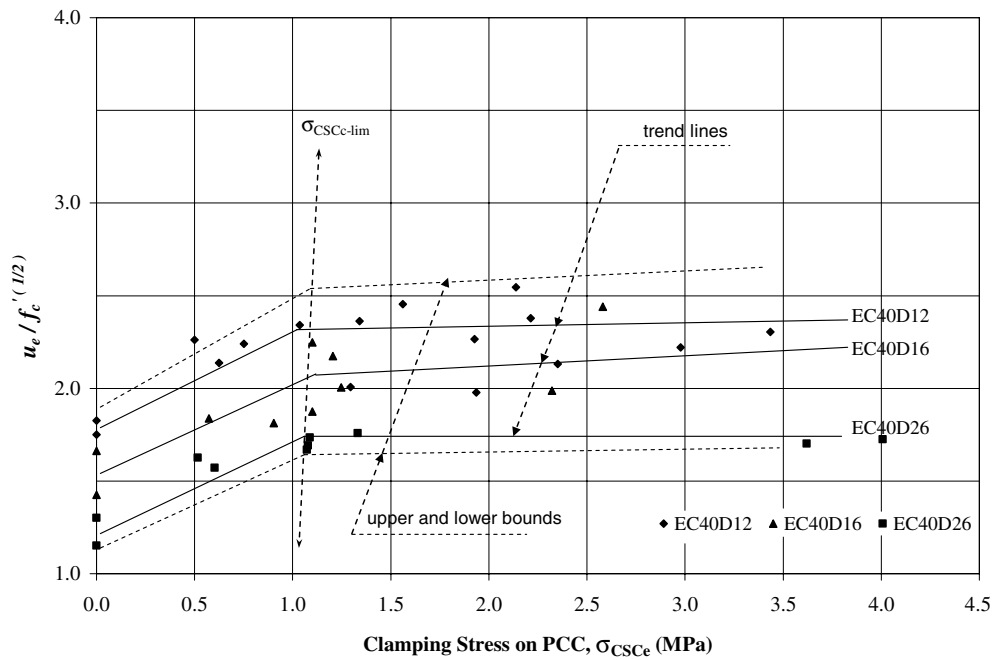


Fig. 5. Normalized bond strength versus clamping stress ($f'_{cn} = 40$ MPa).

crete lugs) of failure. The change in failure mode from one to another is gradual and the limiting clamping stress points out the border between the splitting failure zone and the zone at which mixed failure (splitting and pull-out) takes place. It was observed that the limiting clamping stress is primarily influenced by the concrete strength and the reinforcing bar diameter as shown in Figs. 4 and 5.

4. Modeling the response

The experimental part of this study revealed that the beneficial effects of the FRP overlays on bond strength enhancement of reinforcing bars, which was presented in Figs. 4 and 5, may be modeled through a bilinear approach as shown in Fig. 6. The horizontal axis of the model is defined as the calculated clamping stress on the pseudo-

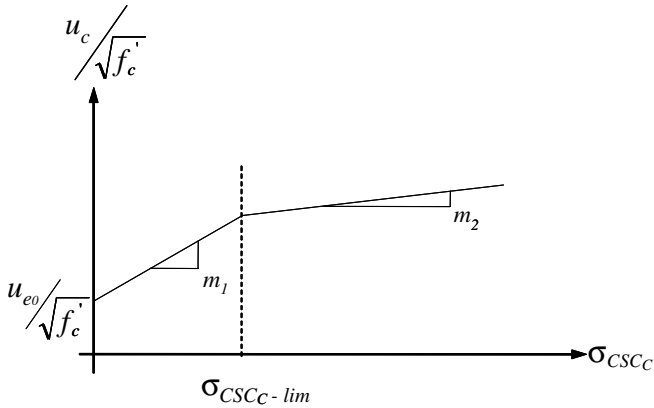


Fig. 6. Idealized effectiveness of FRP clamping on bond strength.

concrete-cylinder, σ_{CSCc} , while the vertical axis shows the calculated normalized bond strength, $u_c / \sqrt{f'_c}$. The change in the effectiveness of the clamping stresses, where the slope of the trend line changes, is called the limiting clamping stress on PCC, $\sigma_{CSCc-lim}$.

4.1. Limit on clamping stress and bond strength enhancement

The limiting clamping stress that controls the effectiveness of the FRP overlay $\sigma_{CSCc-lim}$ (Fig. 6) is primarily related to, and also a function of, the concrete compressive strength and the reinforcing bar diameter as given in Eq. (5)

$$\sigma_{CSCc-lim} = 1 + \left[(7.07 - \sqrt{f'_c}) \frac{k_1}{D_b} \right] \quad (5)$$

where the aspect coefficient, k_1 is used to consider the perimeter over area relation of different reinforcing bar

sizes. The aspect coefficient, k_1 is graphically presented in Fig. 7. Linear interpolation is possible for the concrete strength classes between the specified values of Fig. 7.

The enhancement in normalized bond strength due to FRP overlays before and after the limiting clamping stress may be modeled by Eqs. (6a) and (6b). The initial slope of the model (Fig. 6) is assumed constant, while the second half of the model has a variable slope depending on the concrete compressive strength

$$\frac{u_c}{\sqrt{f'_c}} = \frac{u_{eo}}{\sqrt{f'_c}} + 0.47\sigma_{CSCc} \quad (\sigma_{CSCc} \leq \sigma_{CSCc-lim}) \quad (6a)$$

$$\frac{u_c}{\sqrt{f'_c}} = \frac{u_{eo}}{\sqrt{f'_c}} + 0.47\sigma_{CSCc-lim} + \left(\frac{1 + 0.1\sqrt{f'_c}}{100} \right) \times (\sigma_{CSCc} - \sigma_{CSCc-lim}) \quad (\sigma_{CSCc} > \sigma_{CSCc-lim}) \quad (6b)$$

It should be recalled that the experimental clamping stress on the PCC, σ_{CSCc} is calculated by using the stress on FRP composite as given in Eq. (4). A through investigation on the test data revealed that the predicted strains on FRP at the time of splitting bond failure (ϵ_{FRPc}) is closely related to the reinforcing bar diameter (D_b), and the modulus of elasticity of the composite overlay; ϵ_{FRPc} is calculated as given in Eq. (7)

$$\epsilon_{FRPc} = \epsilon_{co} + 0.0004 \left[\frac{D_b^2 n t_{FRP} E_{Comp}}{4 \times 10^6} \right] \quad (7)$$

where the concrete surface strain for the unconfined specimens at the time of bond failure assumed constant for all specimens; $\epsilon_{co} = 0.0012$.

The clamping stress developed by FRP overlay is calculated as shown in Eq. (8). The numerical result of Eq. (8)

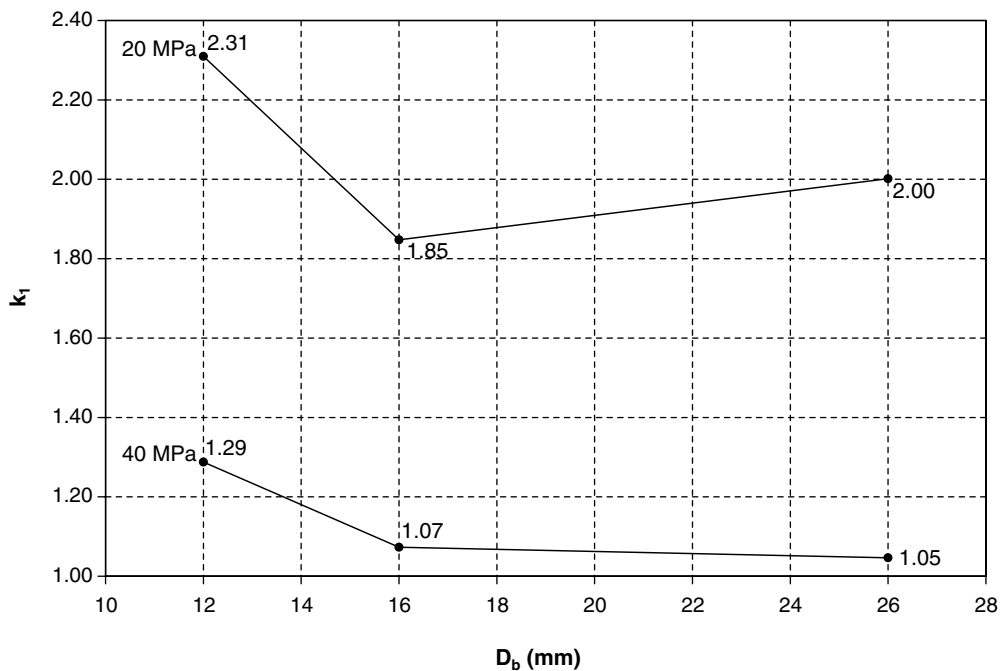


Fig. 7. Aspect coefficient, k_1 for the proposed model.

Table 4
Comparison of experimental results with the proposed model

Specimen	(1) $u_e/f_c^{(1/2)}$	(2) k_1	(3) $\sigma_{CSCc-lim}$ (MPa)	(4) σ_{CSCc} (MPa)	(5) $\Delta(u_e/f_c^{(1/2)})$	(6) $u_e/f_c^{(1/2)}$	(1/6) $(u_e/f_c^{(1/2)})/(u_e/f_c^{(1/2)})$
1 EC20D12-F00-A	2.13	–	–	–	–	–	–
2 EC20D12-F00-B	–	–	–	–	–	–	–
3 EC20D12-FC2-A	2.52	2.24	1.46	1.29	0.61	2.74	0.92
4 EC20D12-FC2-B	2.43	2.23	1.45	1.29	0.61	2.74	0.89
5 EC20D12-FC4-A	2.92	2.24	1.46	3.24	0.71	2.84	1.03
6 EC20D12-FC4-B	3.13	2.23	1.45	3.24	0.71	2.84	1.10
7 EC20D12-FG3-A	2.84	2.24	1.46	0.76	0.36	2.49	1.14
8 EC20D12-FG3-B	2.83	2.23	1.45	0.76	0.36	2.49	1.14
9 EC20D12-FG5-A	2.62	2.24	1.46	1.42	0.67	2.80	0.94
10 EC20D12-FG5-B	2.55	2.23	1.45	1.42	0.67	2.80	0.91
11 EC20D16-F00-A	1.67	–	–	–	–	–	–
12 EC20D16-F00-B	–	–	–	–	–	–	–
13 EC20D16-FC2-A	2.54	1.80	1.27	1.16	0.55	2.22	1.14
14 EC20D16-FC2-B	2.15	1.79	1.27	1.16	0.55	2.22	0.97
15 EC20D16-FC2-r	2.23	1.88	1.31	1.16	0.55	2.22	1.00
16 EC20D16-FC4-A	2.21	1.80	1.27	3.21	0.63	2.30	0.96
17 EC20D16-FC4-B	2.36	1.79	1.27	3.21	0.63	2.30	1.03
18 EC20D16-FC4-r	2.33	1.88	1.31	3.21	0.64	2.31	1.01
19 EC20D16-FG3-A	2.05	1.80	1.27	0.65	0.31	1.98	1.04
20 EC20D16-FG3-B	1.93	1.79	1.27	0.65	0.31	1.98	0.97
21 EC20D16-FG5-A	2.57	1.80	1.27	1.29	0.60	2.27	1.13
22 EC20D16-FG5-B	2.03	1.79	1.27	1.29	0.60	2.27	0.89
23 EC20D16-FG5-r	2.40	1.88	1.31	1.29	0.61	2.28	1.05
24 EC20D26-F00-A	1.43	–	–	–	–	–	–
25 EC20D26-F00-B	–	–	–	–	–	–	–
26 EC20D26-FC2-A	1.89	1.78	1.14	1.16	0.54	1.97	0.96
27 EC20D26-FC2-B	1.84	1.94	1.18	1.16	0.55	1.98	0.93
28 EC20D26-FC4-A	2.19	1.78	1.14	3.76	0.57	2.00	1.10
29 EC20D26-FC4-B	2.01	1.94	1.18	3.76	0.59	2.02	1.00
30 EC20D26-FC4-r	2.00	2.03	1.21	3.76	0.61	2.04	0.98
31 EC20D26-FG3-A	1.81	1.78	1.14	0.59	0.28	1.71	1.06
32 EC20D26-FG3-B	1.91	1.94	1.18	0.59	0.28	1.71	1.12
33 EC20D26-FG5-A	1.93	1.78	1.14	1.31	0.54	1.97	0.98
34 EC20D26-FG5-r	2.07	2.03	1.21	1.31	0.57	2.00	1.04
35 EC40D12-F00-A-r	1.79	–	–	–	–	–	–
36 EC40D12-F00-B-r	–	–	–	–	–	–	–
37 EC40D12-FC2-A	2.13	1.18	1.06	1.29	0.50	2.29	0.93
38 EC40D12-FC2-A-r	2.24	1.05	1.03	1.29	0.49	2.28	0.98
39 EC40D12-FC2-B	2.01	1.01	1.03	1.29	0.49	2.28	0.88
40 EC40D12-FC2-B-r	2.36	1.24	1.07	1.29	0.51	2.30	1.03
41 EC40D12-FC4-A	2.22	1.18	1.06	3.24	0.53	2.32	0.96
42 EC40D12-FC4-A-r	2.30	1.05	1.03	3.24	0.52	2.31	1.00
43 EC40D12-FC4-B	2.55	1.01	1.03	3.24	0.52	2.31	1.10
44 EC40D12-FC4-B-r	2.45	1.24	1.07	3.24	0.54	2.33	1.05
45 EC40D12-FG3-A-r	2.26	1.05	1.03	0.76	0.36	2.15	1.05
46 EC40D12-FG3-B-r	2.14	1.24	1.07	0.76	0.36	2.15	1.00
47 EC40D12-FG5-A	2.38	1.18	1.06	1.42	0.50	2.29	1.04
48 EC40D12-FG5-A-r	1.98	1.05	1.03	1.42	0.49	2.28	0.87
49 EC40D12-FG5-B	2.27	1.01	1.03	1.42	0.49	2.28	1.00
50 EC40D12-FG5-B-r	2.34	1.24	1.07	1.42	0.51	2.30	1.02
51 EC40D16-F00-A	1.54	–	–	–	–	–	–
52 EC40D16-F00-B	–	–	–	–	–	–	–
53 EC40D16-FC2-A	2.25	1.05	1.05	1.16	0.50	2.04	1.10
54 EC40D16-FC2-B	1.87	0.96	1.03	1.16	0.49	2.03	0.92
55 EC40D16-FC4-A	2.44	1.05	1.05	3.21	0.53	2.07	1.18
56 EC40D16-FC4-B	1.99	0.96	1.03	3.21	0.52	2.06	0.97
57 EC40D16-FG3-A	1.84	1.05	1.05	0.65	0.31	1.85	0.99
58 EC40D16-FG3-B	1.81	0.96	1.03	0.65	0.31	1.85	0.98
59 EC40D16-FG5-A	2.00	1.05	1.05	1.29	0.50	2.04	0.98
60 EC40D16-FG5-B	2.17	0.96	1.03	1.29	0.49	2.03	1.07
61 EC40D26-F00-A	1.23	–	–	–	–	–	–
62 EC40D26-F00-B	–	–	–	–	–	–	–
63 EC40D26-FC2-A	1.76	0.88	1.02	1.16	0.48	1.71	1.03

Table 4 (continued)

Specimen	(1) $u_e/f_c^{(1/2)}$	(2) k_1	(3) $\sigma_{CSCc-lim}$ (MPa)	(4) σ_{CSCc} (MPa)	(5) $\Delta(u_e/f_c^{(1/2)})$	(6) $u_e/f_c^{(1/2)}$	(1/6) $(u_e/f_c^{(1/2)})/(u_e/f_c^{(1/2)})$	
64	EC40D26-FC2-B	1.67	0.80	1.01	1.16	0.48	1.71	0.98
65	EC40D26-FC4-A	1.73	0.88	1.02	3.76	0.52	1.75	0.99
66	EC40D26-FC4-B	1.70	0.80	1.01	3.76	0.52	1.75	0.97
67	EC40D26-FG3-A	1.63	0.88	1.02	0.59	0.28	1.51	1.08
68	EC40D26-FG3-B	1.57	0.80	1.01	0.59	0.28	1.51	1.04
69	EC40D26-FG5-A	1.73	0.88	1.02	1.31	0.48	1.71	1.01
70	EC40D26-FG5-B	1.69	0.80	1.01	1.31	0.48	1.71	0.99

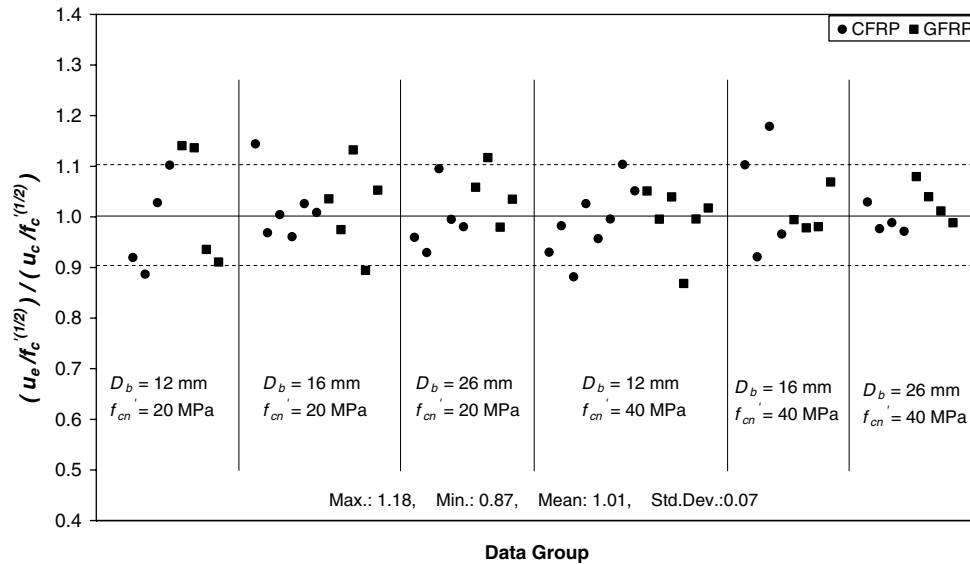


Fig. 8. Comparison of the proposed model with the experimental data.

need to be compared with the limiting clamping stress (Eq. (5)) before calculating the bond strength enhancement according to Eq. (6a) or Eq. (6b)

$$\sigma_{CSCc} = \frac{(\varepsilon_{FRPc} E_{Comp}) n t_{FRP}}{3D_b} \quad (8)$$

4.2. Model predictions versus test data

The normalized test data and model predictions of the 70 eccentric pullout specimens, with or without FRP overlays, are also given in Table 4. The experimental versus calculated values for the normalized results, with a mean value of 1.01 and a standard deviation of 0.07, are graphically presented in Fig. 8. Although the model predictions have more or less the same level of accuracy for different variable groups (Fig. 8), calculated values yielded better correlation for the specimens with larger bar diameters. This effect may be attributed to the higher relative rib area of $D_b = 26$ mm diameter reinforcing bars (Table 1), that results in higher radial stresses and disturbance on the PCC.

5. Conclusions

This paper presents the experimental results of a research on the effect of FRP wrapping on bond strength enhancement of single reinforcing bars embedded in NSC. All specimens were designed and constructed with insufficient anchorage length and small cover thickness equal to reinforcing bar diameter. The following conclusions are drawn based mainly on the results of the current study. It should be noted that, more comprehensive predictions and design equations on the member response and bond strength enhancement may be obtained with further investigations incorporating several other variables.

- FRP wrapping resulted in bond strength enhancement in all specimens regardless of the concrete strength, bar diameter and the type and number of layers of FRP overlay.
- The orientation and number of the splitting cracks in radial direction, starting from the reinforcing bar and ending at the nearest concrete free surface, are altered by the application of FRP overlays. A single and vertical crack on specimen's cross-section led the non-wrapped

- specimens to failure, while two radial cracks forming a V-notch are observed at the time of failure of the FRP wrapped specimens. The V-notch angle is mainly affected by the clamping force resulted from the FRP wrapping; the effective the FRP wrapping the bigger the V-notch angle.
3. All specimens of the current investigation, wrapped or non-wrapped, failed by splitting type of bond failure.
 4. The bond strength enhancement is closely related to the type and the number of layers of the FRP overlays. It is observed that the bond strength enhancement for the same FRP application is higher in the case of larger bar diameters.
 5. It is believed that the use of FRP overlays improve the small concrete cover thickness and anchorage length deficiencies by means of strengthening the pseudo-concrete-cylinder, PCC.
 6. It can be concluded that the level of bond strength enhancement through FRP wrapping is related to a dependent variable named σ_{CSCe} , which is the clamping stress on the pseudo-concrete-cylinder, PCC.
 7. Although successive increases in the number of layers of FRP or the modulus of elasticity of the FRP overlay result in an increase in σ_{CSCe} , the enhancement in bond strength beyond a limiting value of the clamping stress, $\sigma_{CSCe-lim}$, is far less than that of the small clamping stresses.
 8. A model is proposed to predict the bond strength enhancement through FRP wrapping, where the section is under combined flexure and shear. It is observed that the model predictions and test results yielded good correlation with the experimental results of the current investigation.

Acknowledgement

The authors gratefully acknowledge the technical support of Kocaeli University Structures Laboratory where all the experiments were conducted and the financial support from The Scientific and Technological Research Council of Turkey, TUBITAK (project ICTAG I-670) and the Scientific Research Fund of Kocaeli University. The authors extend their thanks to EKON, FIBROTEK and EPOKIM companies for the supply of FRP and epoxy.

References

- [1] Abrams DA. Tests of bond between concrete and steel. Bulletin No 71, University of Illinois, Urbana, 1913.
- [2] Lutz LA, Gergely P. Mechanics of bond and slip of deformed bars in concrete. ACI J 1967(November):711–21. Proceedings, Title No 64-62.
- [3] Goto Y. Cracks formed in concrete around deformed tension bars. ACI J 1971(April):244–51. Proceedings, Title No 68–26.
- [4] Orangun CO, Jirsa JO, Breen JE. A reevaluation of test data on development length and splices. ACI J 1977(March):114–22. Proceedings, Title No 74–11.
- [5] Thompson MA, Jirsa JO, Breen JE, Meinheit DF. Behavior of multiple lap splices in wide sections. ACI J 1979(February):227–48. Proceedings, Title No 76–12.
- [6] CEB-Task Group Bond Models. Bond of Reinforcement in Concrete – State of Art Report. International Federation for Structural Concrete (fib), Switzerland, 2000.
- [7] Altowaiji WAK, Darwin D, Donahey RC. Bond of reinforcement to revibrated concrete. ACI J 1986(November/December):1035–42. Title No 83–94.
- [8] Jeanty PR, Mitchell D, Mirza MS. Investigation of top bar effects in beams. ACI Struct J 1988(May/June):251–7. Title No 85-S26.
- [9] Darwin D, McCabe SL, Idun EK, Schoenekase SP. Development length criteria: bars not confined by transverse reinforcement. ACI Struct J 1992(November/December):709–20. Title No 89-S68.
- [10] Azizinamini A, Stark M, Roller JJ, Ghosh SK. Bond performance of reinforcing bars embedded in high-strength concrete. ACI Struct J 1993(September/October):555–61. Title No 90-S57.
- [11] Hwang S, Lee Y, Lee C. Effect of silica fume on the splice strength of deformed bars of high-performance concrete. ACI Struct J 1994(May/June):294–302. Title No 91-S29.
- [12] Harajli MH, Hout M, Jalkh W. Local bond stress – slip behavior of reinforcing bars embedded in plain and fiber concrete. ACI Mater J 1995(July/August):343–54. Title No 92-M37.
- [13] Harajli MH, Salloukh KA. Effect of fibers on development/splice strength of reinforcing bars in tension. ACI Mater J 1997(July/August):317–24. Title No 94-M38.
- [14] Hota S, Naaman AE. Bond stress – slip response of reinforcing bars embedded in FRC matrices under monotonic and cyclic loading. ACI Struct J 1997(September/October):525–37. Title No 94-S48.
- [15] Fu X, Chung DDL. Improving the bond strength between steel rebar and concrete by increasing the water/cement ratio. Cem Concr Res 1997;27(12):1805–9.
- [16] Esfahani MR, Rangan BV. Local bond strength of reinforcing bars in normal strength and high-strength concrete (HSC). ACI Struct J 1998(March/April):96–106. Title No 95-S10.
- [17] Azizinamini A, Pavel R, Hatfield E, Ghosh SK. Behavior of lap-spliced reinforcing bars embedded in high-strength concrete. ACI Struct J 1999(September/October):826–35. Title No 96-S91.
- [18] Yerlici V, Özturan T. Factors affecting anchorage bond strength in high-performance concrete. ACI Struct J 2000(May/June):499–507. Title No 97-S54.
- [19] Hamad BS, Harajli MH, Jumaa G. Effect of fiber reinforcement on bond strength of tension lap splices in high-strength concrete. ACI Struct J 2001(September/October):638–47. Title No 98-S61.
- [20] Chan YW, Chen YG, Liu YS. Effect of consolidation on bond of reinforcement in concrete of different workabilities. ACI Mater J 2003(July/August):294–301. Title No 100-M35.
- [21] Untrauer RE, Warren GE. Stress development of tension steel in beams. ACI J 1977(August):368–72. Proceedings, Title No 74-.36, p. 368–72.
- [22] Darwin D, Graham EK. Effect of deformation height and spacing on bond strength of reinforcing bars. ACI Struct J 1993(November/December):646–57. Title No 90-S65.
- [23] Hamad BS. Bond strength improvement of reinforcing bars with specially designed rib geometries. ACI Struct J 1995(January/February):3–13. Title No 92-S1.
- [24] Darwin D, Tholen ML, Idun EK, Zuo J. Splice strength of high relative rib area reinforcing bars. ACI Struct J 1996(January/February):95–107. Title No 93-S10.
- [25] Walker PR, Batayneh MK, Regan PE. Measured and design bond strengths of deformed bars, including the effect of lateral compression. Mag Concr Res 1999;51(1):13–26.
- [26] Zuo J, Darwin D. Splice strength of conventional and high relative rib area bars in normal and high-strength concrete. ACI Struct J 2000(July/August):630–41. Title No 97-S65.
- [27] Kemp EL. Bond in reinforced concrete: behavior and design criteria. ACI J 1986(January/February):50–7. Title No 83-7.

- [28] Fu X, Chung DDL. Effect of corrosion on the bond between concrete and steel rebar. *Cem Concr Res* 1997;27(12):1811–5.
- [29] Einea A, Yehia S, Tadros MK. Lap splices in confined concrete. *ACI Struct J* 1999(November/December):947–55. Title No 96-S104.
- [30] Esfahani MR, Rangan BV. Influence of transverse reinforcement on bond strength of tensile splices. *Cem Concr Compos* 2000;22:159–63.
- [31] Hamad BS, Rteil AA, Soudki KA. Bond strength of tension lap splices in high-strength concrete beams strengthening with glass fiber reinforced polymer wraps. *ASCE J Compos Construct* 2004;8(1):14–21.
- [32] Hamad BS, Rteil AA, Salwan BR, Soudki KA. Behavior of bond-critical regions wrapped with fiber-reinforced polymer sheets in normal and high-strength concrete. *ASCE J Compos Construct* 2004;8(3):248–57.
- [33] Hamad BS, Hage AAY, Harajli MH. Effect of fiber-reinforced polymer confinement on bond strength of reinforcement in beam anchorage specimens. *ASCE J Compos Construct* 2005;9(1):44–51.
- [34] Akpınar E. Upgrading the bond strength of rebars embedded in normal strength concrete by CFRP confinement. MSc thesis, Kocaeli University, Faculty of Engineering, Department of Civil Engineering, 2004. 168p (in Turkish).

Construction and Building MATERIALS

Volume 21

Number 7

July 2007

- 1377 **Effect of confining FRP overlays on bond strength enhancement**
S. Ozden and E. Akpinar
- 1390 **Confidence intervals of prediction and synthesis of prediction estimates for deformability of expanded polystyrene in long-term compression**
I. Gnip, V. Keršulis, S. Vaitkus and S. Vėjelis
- 1399 **Evaluation of the sulfate resistance of concrete containing palm oil fuel ash**
C. Jaturapitakkul, K. Kiattikomol, W. Tangchirapat and T. Saeting
- 1406 **Fuzzy logic modeling of deflection behavior against dynamic loading in flexible pavements**
M. Saltan, S. Saltan and A. Şahiner
- 1415 **Reduction of the lateral thrust of masonry arches and vaults with FRP composites**
L. De Lorenzis, R. Dimitri and A. La Tegola
- 1431 **Strength of carbon fiber reinforced polymers bonded to concrete and masonry**
U.S. Camli and B. Binici
- 1447 **Mechanical behavior of corroded reinforcing steel bars S500s tempcore under low cycle fatigue**
Ch. Alk. Apostolopoulos
- 1457 **The effect of potassium carbonate, borax and wolmanit on the burning characteristics of oriented strandboard (OSB)**
K. Ozkaya, A.C. Ilce, E. Burdurlu and S. Aslan
- 1463 **Effects of type and dosage of alkaline activator and temperature on the properties of alkali-activated slag mixtures**
V. Živica
- 1470 **Resilient behavior of compacted subgrade soils under the repeated triaxial test**
D. Kim and J.R. Kim
- 1480 **Study on lime-fly ash-phosphogypsum binder**
W. Shen, M. Zhou and Q. Zhao

Continued on inside back cover

This journal is listed in *SCI Abstracts, Science Citation Index, CAB Abstracts, Concrete Abstracts, Compendex and Engineering Index, Materials Science Citation Index and Research Alert*. Also covered in the abstract and citation database SCOPUS®. Full text available on ScienceDirect®.



0950-0618(200707)21:7;1-H

3017



Volume 21, Number 7, July 2007

ISSN 0950-0618

Construction and Building MATERIALS

*An International Journal
Dedicated to the Investigation
and Innovative Use of
Materials in Construction
and Repair*

Available online at www.sciencedirect.com

 ScienceDirect

Construction and Building MATERIALS

EDITOR-IN-CHIEF

Professor M C Forde
School of Civil and Environmental
Engineering
Kings Buildings
University of Edinburgh
Edinburgh EH9 3JL
Scotland, UK

REGIONAL EDITORS

Professor L Binda
Dept of Structural Engineering
Politecnico di Milano
Piazza L. da Vinci, 32
20133 Milano
Italy

Professor M Ohtsu
Dept of Civil & Environmental
Engineering
Kumamoto University
Kurokami 2-39-1
Kumamoto 860
Japan

EDITORIAL ADVISORY BOARD

M Basheer, *Queens University,
Belfast, UK*

J H Bungey, *University of Liverpool,
Liverpool, UK*

O Buyukozturk, *Massachusetts Institute
of Technology, Cambridge,
MA, USA*

M Y L Chew, *National University of Singapore,
Singapore*

D M Frangopol, *Lehigh University, Bethlehem,
PA, USA*

P E Grattan-Bellew, *Materials & Petrographic
Research G-B Inc, Ottawa,
ON, Canada*

D van Gemert, *Katholieke Universiteit
Leuven, Heverlee, Belgium*

P C Hewlett, *British Board of
Agrément, Watford, UK*

K C Hover, *Cornell University Ithaca, NY, USA*

C K Y Leung, *Hong Kong University of
Sciences & Technology, Hong Kong, China*

P B Lourenço, *University of Minho, Azurém,
Portugal*

V M Malhotra, *CANMET, Ottawa, Canada*

J Mirza, *Hydro-Quebec, Varennes, Canada*

T R Naik, *University of Wisconsin,
Milwaukee, WI, USA*

A S Nowak, *University of Michigan,
Ann Arbor, MI, USA*

Y Ohama, *Nihon University, Koriyama,
Japan*

S Rizkalla, *North Carolina State University,
NC, USA*

P P Rossi, *R teknos, Bergamo,
Italy*

N G Shrive, *University of Calgary,
Alberta, Canada*

Jin-Guang Teng, *Hong Kong Polytechnic
University, Hong Kong, China*

T Tomiita, *Ministry of Construction,
Tsukuba City, Japan*

G F True, *GFT Materials Consultancy,
Dudley, UK*

H G Wheat, *University of Texas at Austin,
Austin, TX, USA*

Construction and Building Materials is an international journal published monthly.

Publishing Office: Elsevier Ltd, The Boulevard, Langford Lane, Kidlington, Oxford OX5 1GB, UK. Phone: (1865) 843000. Fax: (1865) 843010.

Publication information: *Construction and Building Materials* (ISSN 0950-0618). For 2007, volume 21 is scheduled for publication. Subscription prices are available upon request from the Publisher or from the Regional Sales Office nearest you or from this journal's website (<http://www.elsevier.com/locate/conbuildmat>). Further information is available on this journal and other Elsevier products through Elsevier's website (<http://www.elsevier.com>). Subscriptions are accepted on a prepaid basis only and are entered on a calendar year basis. Issues are sent by standard mail (surface within Europe, air delivery outside Europe). Priority rates are available upon request. Claims for missing issues should be made within six months of the date of dispatch.

Advertising information. Advertising orders and enquiries can be sent to: **USA, Canada and South America:** Mr Tino DeCarlo, The Advertising Department, Elsevier Inc., 360 Park Avenue South, New York, NY 10010-1710, USA; phone: (+1) (212) 633 3815; fax: (+1) (212) 633 3820; e-mail: t.decarlo@elsevier.com. **Europe and ROW:** Katrina Barton, Advertising Department, Elsevier Ltd, 84 Theobald's Road, London WC1X 8RR, UK; phone (+44) 207 611 4117; fax: (+44) 207 611 4463; e-mail: k.barton@elsevier.com

Orders, claims, and journal enquiries: please contact the Customer Service Department at the Regional Sales Office nearest you: **Orlando:** Elsevier, Customer Service Department, 6277 Sea Harbor Drive, Orlando, FL 32887-4800, USA; phone: (877) 8397126 or (800) 6542452 [toll free numbers for US customers]; (+1) (407) 3454020 or (+1) (407) 3454000 [customers outside US]; fax: (+1) (407) 3631354 or (+1) (407) 3639661; e-mail: usjcs@elsevier.com or elspcs@elsevier.com. **Amsterdam:** Elsevier, Customer Service Department, PO Box 211, 1000 AE Amsterdam, The Netherlands; phone: (+31) (20) 4853757; fax: (+31) (20) 4853432; e-mail: nlinfo-f@elsevier.com. **Tokyo:** Elsevier, Customer Service Department, 4F Higashi-Azabu 1-Chome Bldg, 1-9-15 Higashi-Azabu, Minato-ku, Tokyo 106-0044, Japan; phone (+81) (3) 5561 5037; fax: (+81) (3) 5561 5047; e-mail: jp.info@elsevier.com. **Singapore:** Elsevier, Customer Service Department, 3 Killiney Road, #08-01 Winsland House I, Singapore 239519; phone: (+65) 63490222; fax: (+65) 67331510; e-mail: asiainfo@elsevier.com

Author enquiries: For enquiries relating to the submission of articles (including electronic submission where available) please visit Elsevier's Author Gateway at <http://authors.elsevier.com>. The Author Gateway also provides the facility to track accepted articles and set up e-mail alerts to inform you of when an article's status has changed, as well as detailed artwork guidelines, copyright information, frequently asked questions and more.

Contact details for questions arising after acceptance of an article, especially those relating to proofs, are provided after registration of an article for publication.